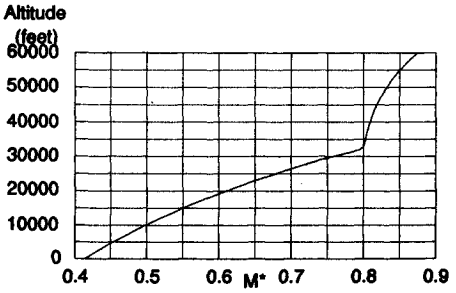

Fig. 1 Best cruise Mach number.

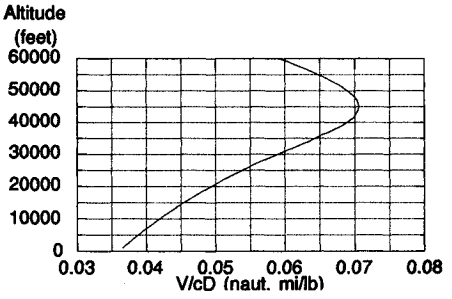

Fig. 2 Best cruise n.mi./lb.

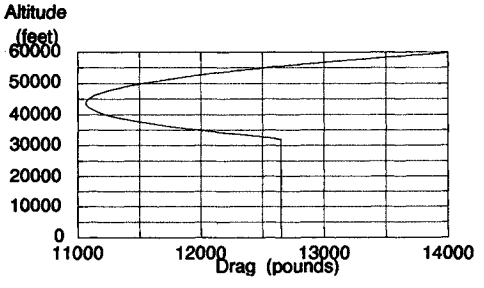

Fig. 3 Drag at best cruise Mach number.

ft where M^* is less than 0.8, q^* is constant. Thus the drag is constant.

The data in these figures does not include the possibility that the aircraft may be thrust limited. If limited, that would preclude the possibility of reaching the global optimum.

The analytical solution is obtained from Eq. (43)

$$M^* = 0.81875$$

The optimal value for the dynamic pressure is

$$q^* = 144.38 \text{ lb/ft}^2$$

$$\sigma = 0.19336$$

Optimal cruise altitude is approximately

$$h^* = 45{,}120 \text{ ft}$$

Conclusions

It has been demonstrated that best cruise speed is in the drag rise region if sufficient thrust is available. Best cruise altitude corresponds to the altitude where drag is a global minimum. These results disprove the theory that the cruise lift to drag ratio is

$$\frac{3^{1/2}}{2}\left(\frac{L}{D}\right)_{\max}$$

where max lift-to-drag ratio is based upon constant aerodynamic drag coefficients; that is prior to drag rise.

References

[1]Anderson, J. N., Jr., *Introduction to Flight*, 3rd ed., McGraw-Hill, New York, 1985.

[2]Nicolai, L. M., "Fundamentals of AIRCRAFT DESIGN," METS, Inc., San Jose, CA, 1984.

[3]Vinh, N. X., "Optimal Trajectories in Atmospheric Flight," *Studies in Astronautics*, Elsevier, New York, 1981.

[4]Perkins, C. D., and Hage, R. E., "Airplane Performance Stability and Control, Wiley, New York, 1949.

[5]Miller, L. E., "Aircraft Flight Performance Methods," rev. 2, AFFDL-TR-75-89, Wright-Patterson AFB, OH, 1978.

Vortex Breakdown Studies of a Canard-Configured X-31A-Like Fighter Aircraft Model

Sheshagiri K. Hebbar* and Max F. Platzer†
Naval Postgraduate School, Monterey, California 93943
and
Hui Man Kwon‡
Korean Air Force, Republic of Korea

Introduction

THE use of canard configurations as a potential method for improved aerodynamic performance has received considerable attention recently, both experimentally and computationally. Since the experimental study by Behrbohm,[1] there have been a number of canard-related investigations.[2] The more recent experimental studies by Er-El and Seginer,[3] Calarese,[4] and Hummel and Oelker[2] focused on the interaction mechanism of canard and wing vortex systems. Considerable progress has also been made in the computation of high angle-of-attack (AOA) flows over delta and double-delta wings, canard-wing combinations,[5] and even complete aircraft configurations, such as the F-18 and X-31 aircraft.[6]

As pointed out in Ref. 2, the flow physics of the canard-wing configuration is still not sufficiently understood and documented. The high AOA flight is limited by the vortex breakdown phenomenon and by the onset of vortex asymmetry. The canards have a strong influence on the vortex development and on the lateral and directional stability. Of special importance is the understanding of the vortex development and breakdown (bursting) under rapidly maneuvering conditions as envisioned for the X-31A aircraft. Therefore, this investigation was undertaken to characterize the vortical flowfield around a maneuvering canard-configured fighter aircraft model comparable to X-31A. It included extensive static and dynamic flow visualization experiments in the 0–50-deg AOA range using dye-injection technique in the Naval Postgraduate School (NPS) water tunnel. Additional details of the investigation appear in Refs. 7 and 8.

Presented as Paper 91-1629 at the AIAA 22nd Fluid Dynamics, Plasmadynamics, and Lasers Conference, Honolulu, HI, July 24–27, 1991; received Aug. 28, 1991; revision received May 14, 1992; accepted for publication May 14, 1992. This paper is declared a work of the U.S. Government and is not subject to copyright protection in the United States.

*Adjunct Professor, Department of Aeronautics and Astronautics. Associate Fellow AIAA.

†Professor, Department of Aeronautics and Astronautics. Associate Fellow AIAA.

‡Major.

Experiment

Water Tunnel Facility and Aircraft Model

The NPS water tunnel is a horizontal, continuous flow, closed circuit facility with a test section measuring 38-cm (15-in.) wide, 51-cm (20-in.) high, and 152-cm (60-in.) long. The model support system attached to the top of the test section utilizes a C-strut to vary the pitch angle travel up to 50 deg, and a turntable to provide yaw variations up to ±20 deg (Fig. 1). Two servo motors provide independent control of model pitch and yaw. The model used in this investigation is a simplified, 2.3% scale model approximating the X-31A fighter aircraft with a double-delta wing, a delta-canard, a rectangular fuselage, and several dye-injection ports (Fig. 2a). The key model dimensions are: total length = 30.5 cm (12 in.), span of wing/canard = 20.3 cm (8 in.)/5.1 cm (2 in.), and root chord of wing/canard = 14.0 cm (5.5 in.)/2.5 cm (1.0 in.).

The modular construction of the fuselage permits changes in horizontal and vertical location of the canard relative to the wing. The canard's horizontal distance X_c and its vertical distance Z_c are measured from the quarter point of the canard root chord to the quarter point of the wing root chord (Fig. 2b). The wing root chord C_{wr} is used to obtain canard's nondimensionalized distances $\bar{X}_c = X_c/C_{wr}$, $\bar{Z}_c = Z_c/C_{wr}$.

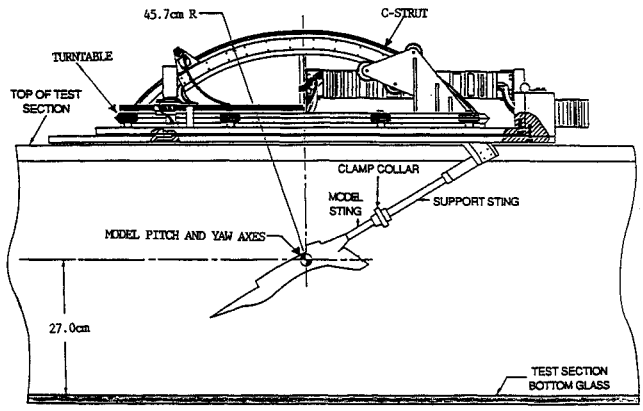

Fig. 1 Model support system of the NPS water tunnel.

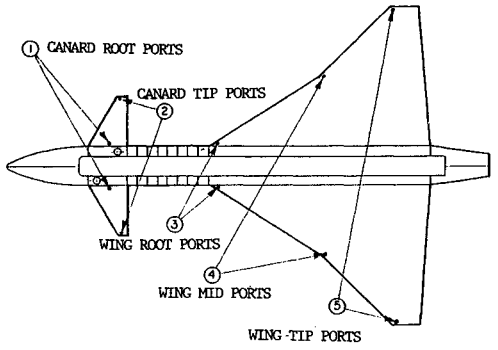

Fig. 2a 2.3% Scale model of X-31A-like aircraft with dye-injection ports.

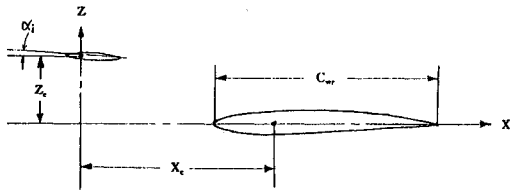

Longitudinal location $\bar{X}_c = X_c/C_{wr}$
Vertical location $\bar{Z}_c = Z_c/C_{wr}$
Incidence angle $\alpha_i = 2^0$

Fig. 2b Description of canard location.

Experimental Program and Test Conditions

The experimental program was carried out in two phases. The first phase involved flow visualization studies to determine the optimum canard location on the X-31A-like model and was carried out for 23 canard locations under static conditions at 0, 15, 20, and 25-deg AOA (α) with zero sideslip angle (β). The second phase involved the dynamic wing vortex visualization of the optimum-configured X-31A-like model with zero sideslip at two pitch rates with AOA varying from 0 to 50 deg (simple pitch-up motion) and 50 to 0 deg (simple pitch-down motion). The flow velocity in the water tunnel was nearly constant at 7.5 cm/s (0.25 ft/s), corresponding to a nominal Reynolds number of 10,200 based on wing root chord. The reduced pitch rates were $k = 0.06$ and 0.17. (Based on the definition given in Ref. 8, the values quoted there for the reduced pitch rate should be corrected to read as $k = 0.03$ and $k = 0.08$.) The reduced pitch rate is defined by $k = \dot{\alpha}L/2U_\infty$ where L is the model length, U_∞ is the freestream velocity, and $\dot{\alpha}$ is the pitch rate in rad/s. The model pitch-axis was located at 62.7% of the wing root chord. Extensive videotape recording and 35-mm photography of the model flowfield in both top view and side view were performed to document the observed flow phenomena during static and dynamic conditions.

Results and Discussion

Data reduction essentially consisted of measuring the burst location of the wing root vortex X_b from the leading edge of the wing root chord. All measurements were made on the starboard side of the model. The burst locations were visually determined from the photographs with the utmost care and consistency, and scaled for nondimensionalization using the wing root chord. For a discussion on the quality of NPS water tunnel burst data, see Hebbar et al.[9]

Effects of Canard Location on Wing Root Vortex Core Breakdown

Figure 3 shows a typical variation of burst location as a function of horizontal position of canard at a fixed vertical distance for three AOAs (15, 20, and 25 deg). It is clear that at 20-deg AOA and above, the vortex burst location moves backward (vortex core length increases) as the canard moves closer to the wing. A slight reduction observed in the vortex

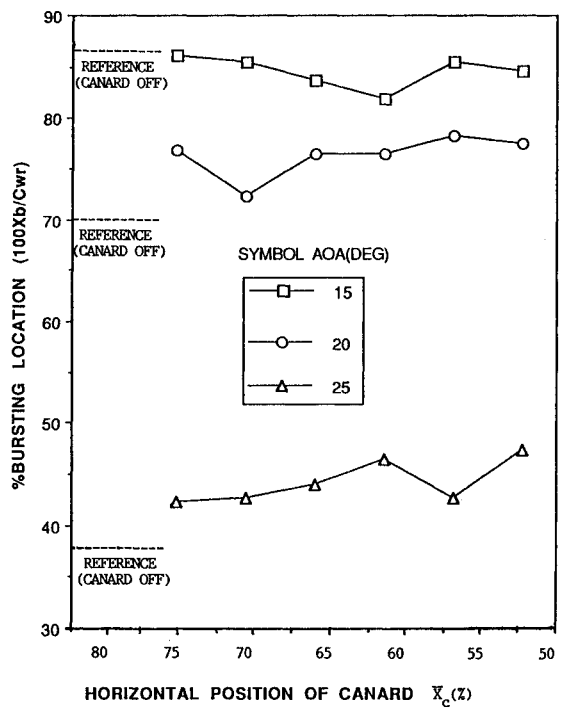

Fig. 3 Wing root vortex burst location as a function of horizontal position of the canard for static case at different AOAs; $\bar{Z}_c$ = 10.23%.

core length at 15-deg AOA is within the estimated experimental uncertainty for the burst location. Figure 4 presents typical burst location plots as a function of the angle of attack for one longitudinal position of the canard but different vertical locations. These plots clearly show that at any given canard location the vortex burst point moves upstream (reducing the core length) as the AOA increases. A close scrutiny of the vortex breakdown characteristics of these plots and others not shown here reconfirmed the well-known fact[2] that a close-coupled, high-canard configuration leads to a favorable aerodynamic interference between the vortical flowfields of the canard and the wing upper surface. On the basis of the vortex burst response the canard location corresponding to $\bar{X}_c = 52.27\%$ and $\bar{Z}_c = 7.95\%$ was judged to be the optimum for the X-31A-like model. The later tests with a closer longitudinal canard location did not indicate any significant improvement in the burst response.

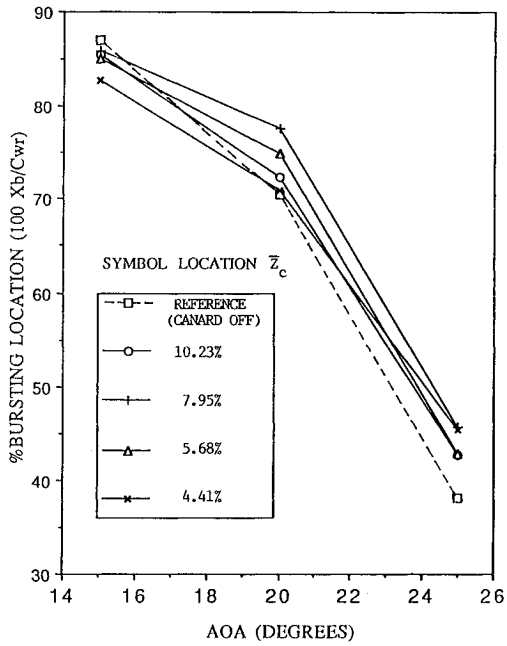

Fig. 4 Wing root vortex burst location as a function of AOA for static case at different vertical locations of the canard; $\bar{X}_c$ = 70.45%.

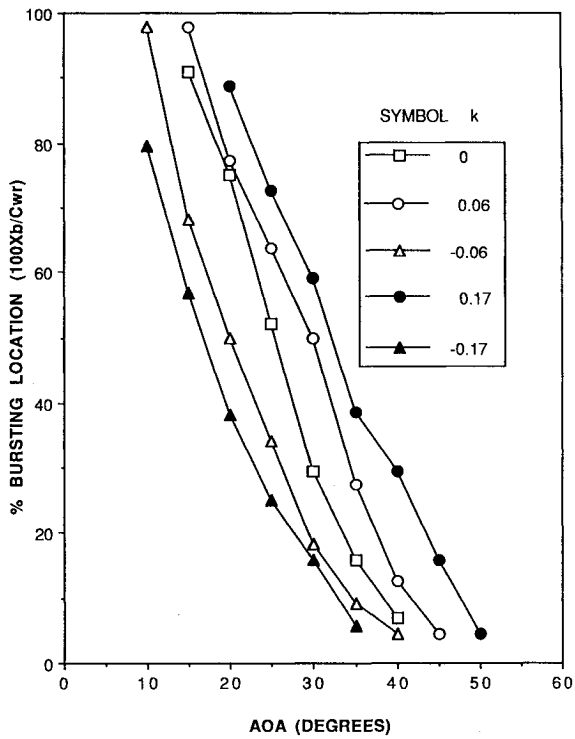

Fig. 5 Wing root vortex burst location for static and dynamic conditions at zero sideslip angle; $\bar{X}_c$ = 52.27%, $\bar{Z}_c$ = 7.95%.

Effects of Angle of Attack on Wing Root Vortex Core Breakdown

Figure 5 presents the burst location plot as a function of the angle of attack for canard location $\bar{X}_c = 52.27\%$, $\bar{Z}_c = 7.95\%$ under static condition with zero sideslip. The flow over the wing remained attached up to about 13-deg AOA where it began to coil up into a tightly wound vortex core on the wing surface, extending aft until undergoing vortex core breakdown downstream of the wing trailing edge. As the AOA was increased further, the vortex core breakdown point progressively moved upstream over the wing surface from the trailing edge to the leading edge, reducing the extent of vortical flowfield over the wing.

The vortex burst response during pitch-up and pitch-down motions at zero sideslip is also documented quantitatively in Fig. 5. The dynamic effects of pitch rate are clearly highlighted in these plots. During a pitch-up motion, vortex bursting occurs at a point further downstream than would occur for static condition resulting in a vortex system which is equivalent to a static system at a reduced angle of attack. During a pitch-down motion, the vortex bursting occurs earlier relative to both the pitch-up motion and the static condition. In the AOA range considered, the burst location curve consistently undershoots the static curve during the pitch-down motion and overshoots during the pitch-up motion, this undershoot/overshoot (i.e., the burst lag) increasing with the pitch rate. The vortex breakdown response observed here for the pitch-up and pitch-down motions is similar to the ones observed by Hebbar et al.[9] in their experimental investigations of LEX vortices shed off a F/A-18 fighter aircraft model.

Conclusions

The first of a kind flow visualization data reported here for a canard-configured X-31A-like aircraft model lead to the following conclusions:

1) A close-coupled, high-canard configuration results in a more favorable aerodynamic interference between the vortex systems of the canard and the wing upper surface.

2) The dynamic tests indicate that the vortex burst lag increases with the pitch rate. That is, the location of the wing root vortex burst point relative to the static case moves rearward with increasing pitch-up motion and forward with increasing pitch-down motion.

Acknowledgments

This work was supported by the Naval Air Development Center, the Naval Air Systems Command and the Naval Postgraduate School. The authors sincerely thank Alan McGuire for helping in the design and fabrication of the X-31A-like model.

References

[1]Behrbohm, H., "Basic Low Speed Aerodynamics of the Short-Coupled Canard Configuration of Small Aspect Ratio," SAAB Aircraft Co., TN-60, Linkoping, Sweden, July 1965.

[2]Hummel, D., and Oelker, H., "Effects of Canard Position on the Aerodynamic Characteristics of a Close-Coupled Canard-Configuration at Low Speed," AGARD CP 465, Oct. 1989, pp. 7.1–7.18; see also, *Journal of Aircraft*, Vol. 26, No. 7, 1989, pp. 657–666.

[3]Er-El, J., and Seginer, A., "Vortex Trajectories and Breakdown on Wing-Canard Configurations," *Journal of Aircraft*, Vol. 22, No. 8, 1985, pp. 641–648.

[4]Calarese, W., "Vortex Interaction Effects on the Lift/Drag Ratio of Close-Coupled Canard-Configurations," AIAA Paper 87-1344, June 1987.

[5]Tu, E. L., "Navier-Stokes Simulation of a Close-Coupled Canard-

Wing-Body Configuration," AIAA Paper 91-0070, Jan. 1991.
[6]Yeh, D. T., George, M. W., Clever, W. C., Tam, C. K., and Woan, C. J., "Numerical Study of the X-31 High Angle-of-Attack Flow Characteristics," AIAA Paper 91-1630, June 1991.
[7]Kwon, H. M., "Water Tunnel Flow Visualization Studies of a Canard-Configured X-31A-Like Fighter Aircraft Model," M.S. Thesis, Naval Postgraduate School, Monterey, CA, Sept. 1990.
[8]Hebbar, S. K., Platzer, M. F., and Kwon, H. M., "Static and Dynamic Water Tunnel Flow Visualization Studies of a Canard-Configured X-31A-Like Fighter Aircraft Model," AIAA Paper 91-1629, June 1991.
[9]Hebbar, S. K., Platzer, M. F., and Cavazos, O. V., "A Water Tunnel Investigation of the Effects of Pitch Rate and Yaw on LEX Generated Vortices of an F/A-18 Fighter Aircraft Model," AIAA Paper 91-0280, Jan. 1991; see also, *Journal of Aircraft*, Vol. 29, No. 4, 1992, pp. 720–723.

Transonic Blade-Vortex Interactions: Noise Reduction

Y. Xue* and A. S. Lyrintzis†
University of Minnesota, Minneapolis, Minnesota 55455

Introduction

At the present time noise in the design of new or modified helicopters is a matter of great concern. Among the several types of helicopter noise, that due to blade-vortex interactions (BVI) is one of the most important. BVI is the aerodynamic interaction of a rotor blade with the trailing vortex system generated by preceding blades. It usually occurs during helicopter descent, or low-speed maneuvers. It is loud, impulsive in character, and tends to dominate the other sources when it occurs. Also, very complicated BVI patterns arise from tilt-rotor aircraft. Interactions generate the most significant noise when they are intrinsically unsteady, as when the vortex is exactly parallel to the blade, or when the vortex is nearly parallel to the blade. For typical helicopter cases the aerodynamics and aeroacoustics of the interactions are intrinsically transonic. In such cases the flow can be initially modeled by two-dimensional unsteady transonic flow.

Two-dimensional transonic BVI was first studied computationally in the near and midfield by George and Chang[1,2] who used the high-frequency transonic small disturbance equation, including regions of convected vorticity. A comprehensive code, VTRAN2, was then developed.[3–5] The vorticity is bilinearly distributed inside a vortex core and branch cuts are introduced in the x direction. The two-dimensional transonic BVI problem was also solved using the small disturbance theory and the more complex Euler and thin-layer Navier Stokes equations (e.g., Refs. 6–8). A direct comparison of the results obtained from the different methods (from small disturbance to Navier Stokes equations) shows that the results are very similar.[9] At great distances from the airfoil the waves become very difficult to follow because of numerical diffusion and dispersion errors, which led us to use the Kirchhoff method. The Kirchhoff method was introduced[3–5] to extend the numerically calculated nonlinear aerodynamic near-field results to the linear acoustic farfield.

Received Oct. 28, 1991; revision received April 20, 1992; accepted for publication April 23, 1992.

*Research Assistant, Aerospace Engineering and Mechanics. Student Member AIAA.
†Assistant Professor, Aerospace Engineering and Mechanics. Member AIAA.

In this note several ideas for reduction of transonic BVI noise are introduced and tested. The model used is the two-dimensional high frequency transonic small disturbance equation with regions of distributed vorticity (VTRAN2 code). The far-field noise signals are obtained by using the Kirchhoff method which extends the numerical near-field aerodynamic results to the linear acoustic three-dimensional far field. The results are shown for the airfoil (NACA64A006) shape modification achieved through the addition to various portions of the airfoil lower surface of cosine or NACA 4-digit shapes of different maximum thickness, which demonstrate the idea of shape modification near the leading edge of BVI noise reduction. Also shown are the results for the splitting vortex model, variations of vortex strength, and increasing angle of attack, which are parameters that can be effective to noise reduction. More details can be found in Ref. 10.

Numerical Method (VTRAN2)

VTRAN2 is a code developed for analyzing the interactions of convected regions of vorticity with airfoils using the transonic small disturbance equation. It is based on the ADI implicit scheme of the LTRAN2 code[11] with the inclusion of the high frequency term and the addition of regions of convected vorticity using the cloud-in-cell and multiple branch-cut approach. The vortex can have a free path (convected by the flow) or a prescribed path (miss distance y_v = const, vortex velocity = U_0). The code was modified[5] to include viscosity and monotone switches.

A (213 × 199) nonuniform mesh is used for the calculations. The computational mesh points are clustered more densely near and in front of the airfoil, and are stretched exponentially from the near airfoil region to about 200 chords from the airfoil in the x and 400 in the y direction. More mesh points are added in the y direction for the more accurate evaluation of the normal derivatives on the Kirchhoff surface. The code has a high vectorization level and the CPU time for each two-dimensional case on a Cray-2 computer is about 5 min for 800 time-marching steps.

The numerical simulation method (VTRAN2 code) introduced above is simple and efficient. It is also able to catch the main features of transonic BVI, which are the shock motions around airfoils. The code was shown to agree well with other, more complex approaches, including Euler and thin-layer Navier-Stokes computations.[9] Thus, we expect that our conclusions will also hold if more accurate Euler/Navier-Stokes predictions are used. Three-dimensionality will, of course, influence the results significantly, since the majority of BVIs take place near the tip. Some of the presented results will hold for three-dimensional cases, but only actual three-dimensional calculations can show that.

Kirchhoff's Method for the Far Field

In the past, acoustic analogy has been used for the evaluation of noise signals. This approach starts from the calculation of the nonlinear near and midfield and the far field is found from surface and volume integrals of near and midfield flow and body surfaces. We should note that there are substantial difficulties in including the nonlinear quadrupole term (which requires second derivatives) to the volume integrals, especially around moving shock surfaces. It should also be noted that in the most recent formulation of Farassat et al.[12] the importance of shocks as a potent source of noise is explained. However, only steady shocks are treated. Therefore, in BVI many investigators use data only on the blade surface, which is a less accurate method since shock wave surfaces are not included in the calculation.

Kirchhoff's method includes the calculation of the nonlinear near and midfield with the far-field solutions found from a linear Kirchhoff formulation evaluated on a surface surrounding the nonlinear field. This method provides an adequate matching between the aerodynamic nonlinear near field and the acoustic linear far field. The full nonlinear equations are